Eur Biophys J (2003) 31: 608–616
DOI 10.1007/s00249-002-0258-7

ARTICLE

M. Długosz · E. Błachut-Okrasińska · E. Bojarska
E. Darżynkiewicz · J.M. Antosiewicz

Effects of pH on kinetics of binding of mRNA-cap analogs by translation initiation factor eIF4E

Received: 30 April 2002 / Accepted: 20 September 2002 / Published online: 31 October 2002
© EBSA 2002

Abstract Stopped-flow spectrofluorimetry and a theoretical method for predicting protonation equilibria in polyelectrolytes were combined in an analysis of the pH dependence of the kinetics of binding of analogues of the 5′-mRNA cap to the cap binding protein eIF4E. The computer simulations and available experimental data indicate that there are two titratable groups in the binding site of the protein and two titratable groups on the ligands directly involved in the binding, in addition to stacking interactions described by other groups. The observed pH dependencies of the rate constants obtained from the stopped-flow experiments are consistent with this finding. In particular, it is concluded that binding of both forms of the cap analogs regarding protonation at the N1 position of the guanine ring is efficient, and the shift to a predominantly protonated form of the ring takes place after formation of the complex.

Keywords Stopped flow · pH dependence · Cap binding protein · Cap analogs · Protonation equilibria

Abbreviations *HEPES*: *N*-(2-hydroxyethyl)piperazine-*N*′-(2-ethanesulfonic acid); · *MES*: 2-(*N*-morpholino)ethanesulfonic acid · m^7; *GMP*: 7-methylguanosine 5′-monophosphate · m^7; *GDP*: 7-methylguanosine 5′-diphosphate · m^7; *GTP*: 7-methylguanosine 5′-triphosphate

Introduction

It is generally recognized that electrostatic interactions constitute one of the most important determinants of binding affinity between ligands and their target receptors. Ionizable groups in biomolecules represent a dominant contribution to the electrostatic potential around these molecules. Their charge state depends on pH and, as a result, ligand-receptor interactions show some degree of pH dependence. Studies of pH dependence are used to elucidate mechanisms of enzyme catalysis (Tipton and Dixon 1979; Cleland 1982; Stivers et al. 1996; Brendskag et al. 1999), as well as protein-ligand (Taylor et al. 2000) and protein-protein (Kitano et al. 1989) recognition.

We here present the pH dependence of the association and dissociation rate constants of murine translation initiation factor eIF4E, associating with three analogs of the 5′-terminal cap in mRNA: 7-methyl-guanosine 5′-mono-, 5′-di-, and 5′-triphosphate (m^7GMP, m^7GDP, and m^7GTP, respectively). The observations are interpreted on the basis of a theoretical method for prediction of protonation equilibria in proteins (Antosiewicz et al. 1996; Briggs and Antosiewicz 1999).

The eIF4E protein is a key participant in the regulation of translation in eukaryotic cells (Sonenberg and Gingras 1998). This protein specifically recognizes the m^7GpppN cap (where p is a phosphate group and N is any nucleoside) of the 5′-terminus of mRNA during initiation of translation processes. Considerable insight into the structural features of recognition of the mRNA cap by the eIF4E protein have been gained from the three-dimensional structures of its complexes with m^7GDP: the crystal structure for murine eIF4E (Marcotrigiano et al. 1997) and a set of solution structures for yeast eIF4E derived from NMR data (Matsuo et al. 1997). The alkylated base is sandwiched between the side chains of two conserved tryptophans (Trp56 and Trp102 in the murine eIF4E). The interaction can be explained in terms of enhancement of π-π stacking enthalpy, because of charge transfer between the electron-deficient 7-methylguanine (which carries a delocalized positive charge secondary to methylation) and the electron-rich indole groups. However, not all details of interactions between polar titratable groups of the protein and the ligand have

M. Długosz · E. Błachut-Okrasińska · E. Bojarska
E. Darżynkiewicz · J.M. Antosiewicz (✉)
Department of Biophysics, Warsaw University,
Warsaw 02-089, Poland
E-mail: jantosi@biogeo.uw.edu.pl
Tel.: +48-22-5540727
Fax: +48-22-5540001

been elucidated. N1 and N2 make hydrogen bonds with the carboxylate oxygen atoms of Glu103. Arg157 and Lys162 make contacts with oxygen atoms of the phosphate groups. It was established that pH 7.6 is optimal for mRNA cap binding and that the pK_a for the N1 proton of m^7GTP is 7.4 (Rhoads et al. 1983). This led to suggestions that the "enolate" form of 7-methylguanine, with N1 deprotonated, may be recognized by eIF4E. On the other hand, the crystal structure data for murine eIF4E and m^7GDP were interpreted as indicating that eIF4E recognizes the keto form of the base (Marcotrigiano et al. 1997). Marcotrigiano and co-workers suggested that presumably the chemical environment provided by the negative charge of Glu103 increases the pK_a of the N1 proton in its eIF4E-bound state. However, the NMR data do not fully support this suggestion, as the imino proton resonance of 7-methylguanine is absent in the complex with yeast eIF4E (Matsuo et al. 1997). It seems therefore desirable to study protonation equilibria in eIF4E-cap analog complexes.

Materials and methods

Reagents and syntheses

All chemicals for sample preparations were of analytical grade, purchased from Roth. The ligands m^7GMP, m^7GDP, and m^7GTP were synthesized according to Darżynkiewicz et al. (1985), and murine eIF4E(28–217) was prepared as described elsewhere (Marcotrigiano et al. 1997).

Stopped-flow measurements

The binding of cap analogs to eIF4E has been followed in a stopped-flow spectrofluorimeter, by measurements of the quenching of intrinsic tryptophan fluorescence of eIF4E (see e.g. Carberry et al. 1989), due to sandwich stacking between 7-methylguanine and two tryptophan indole rings (Marcotrigiano et al. 1997; Matsuo et al. 1997).

Stopped-flow kinetic measurements were run on a SX.18MV stopped-flow reaction analyser (Applied Photophysics). Emission of eIF4E was excited at 290 nm, with slit widths of 0.5 mm, equivalent to spectral widths of 2.3 nm, and the fluorescence of the protein was monitored after passage through a 320 nm cut-off filter (Applied Photophysics). Absorption and emission path lengths in the stopped-flow cell were 2 mm and 10 mm, respectively. The investigated reactions were initiated by mixing equal volumes of defined concentrations of eIF4E (0.5–1.5 μM) and the cap analog (0.5–18.0 μM) at 20 °C, ionic strength equivalent to 150 mM of the monovalent salt, and the pH in the range 5.2–8.0. The measurements between pH 6.8 and 8.0 were performed in 50 mM HEPES-KOH buffer and those in the pH range 5.2–6.8 using 50 mM MES-KOH buffer. The solutions were filtered prior to concentration determination, and subsequently degassed before placing them into the stopped-flow syringes. One thousand data points were recorded over the course of each reaction using an oversampling option of the instrument, and 28 runs were averaged for each concentration of the reagents. For each pH value the experiment was repeated 2–3 times with protein samples from separate preparations. Concentrations of the reagents were determined spectrophotometrically using $\epsilon_{280} = 53{,}400\ M^{-1}\ cm^{-1}$ for the protein and $\epsilon_{280} = 14{,}000\ M^{-1}\ cm^{-1}$ for the cap analogs at pH 7.2. Solutions of the ligand at higher values of pH were prepared just prior to measurement, to avoid effects of imidazole ring opening under basic conditions (Darżynkiewicz et al. 1988).

Analysis of kinetic transients

Kinetic traces registered by our stopped-flow spectrometer for one pH value and several protein:ligand concentration ratios were simultaneously subjected to nonlinear least-squares regression, assuming a one-step mechanism for the association:

$$P + L \underset{k_D}{\overset{k_R}{\rightleftharpoons}} C \qquad (1)$$

using methods described elsewhere (Długosz et al. 2002); k_R is the bimolecular association rate constant, and k_D is the dissociation rate constant. In principle, when a protein binds a single ligand molecule, a two-step model for binding kinetics would seem more appropriate. This is because it seems reasonable to suggest that there is always some rearrangement of the protein-ligand complex following the initial collision, which leads to at least a two-step binding kinetics (Johnson 1992). However, the observed association processes are very fast and it appeared too difficult to obtain four rate constants characterizing such a mechanism with accuracy sufficient to discuss their pH dependence.

Analysis of pH dependence of the rate constants

Kinetic data obtained from stopped-flow experiments were analysed assuming a single-step association mechanism between different protonation forms of the binding site of the protein and the ligand. Each cap analog considered in the present work possesses two sites titrating in the pH region considered here. One is the N1 atom on the 7-methylguanine, and the other is the terminal phosphate group of the nucleotide with its secondary ionization. The pK_a of N1 in free m^7GMP was determined spectrophotometrically as 7.24 ± 0.03 at 20 °C at an ionic strength corresponding to 150 mM of monovalent salt (Wieczorek et al. 1995). For m^7GTP, the pK_a of N1 is 7.4 (Rhoads et al. 1983). Therefore for m^7GDP the pK_a of N1 can be assumed to be equal to 7.3. Regarding the secondary ionization of the terminal phosphate group of the cap analogs, the only published data give 6.15 for m^7GMP, to be compared to 6.38 for GMP (Darżynkiewicz et al. 1988). On the other hand, the pK_a values, published elsewhere, for secondary phosphate ionization in guanosine mono-, di-, and triphosphates are 6.66, 7.19, and 7.65, respectively (Saenger 1984). Therefore, we assume that the pK_a values for the methylated derivatives can be approximated as 6.5, 7.0, and 7.5, respectively.

Crystal structure data (Marcotrigiano et al. 1997) indicate that m^7GDP bound to the eIF4E protein has direct contacts with the following three titratable residues: Glu103, Arg157, and Lys162. Usually the pK_a values of the side chains of arginine residue are well above the pH region considered in the present work. However, pK_a values for Glu103 and Lys162 are likely to be within this pH range, because the molecular environment of the protein can substantially change the pK_a corresponding to a free group in aqueous medium. Therefore, we can assume that the eIF4E protein contains two titratable residues within its binding site, and consequently the association between cap analogs and the eIF4E is considered as an association between two dibasic acids. The corresponding reaction scheme is shown in Fig. 1. PH_2, PH, and P signify the protein with two, one, and no protons in its binding site. Similarly, LH_2, LH, and L signify the cap analog with two, one, and no protons on its N1 and/or P positions. Each form of the protein is assumed to be able to complex with each form of the cap analog, with different forward (k_R^i) and backward (k_D^i) rate constants, because of the differences in electrostatic interactions. Some microscopic details are neglected, e.g. PH microscopically represents one of the two forms of monoprotonated eIF4E at its binding site, one at Glu103 and the other at Lys162. The reaction model presented in Fig. 1 implicitly assumes that protonation/deprotonation reactions come to equilibrium on a time scale much faster than the protein-ligand association/dissociation reactions, as is usually done for analysis of the effects of pH on enzymes (Tipton and Dixon 1979; Adams and Taylor 1993; Stivers et al. 1996; Taylor et al. 2000).

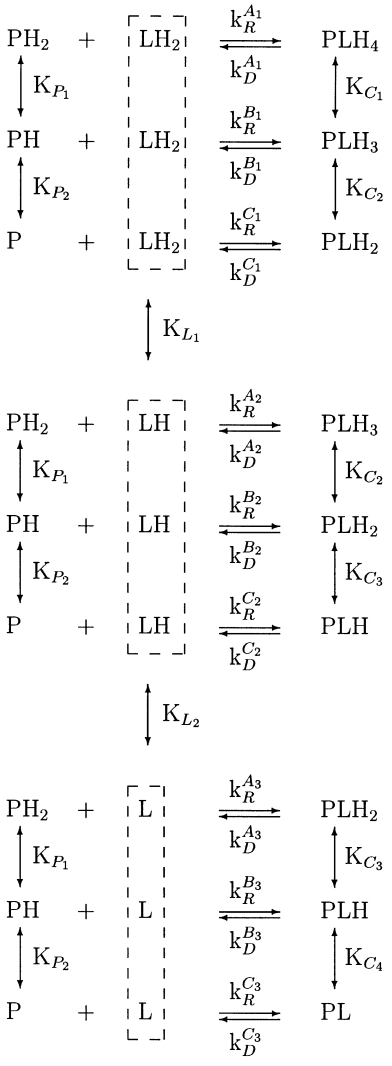

Fig. 1 Proposed mechanism for binding of analogs of the 5′-terminus of mRNA to the eIF4E protein

Proton dissociation constants are defined as:

$$\begin{aligned} K_{\mathrm{P}_1} &= \frac{[\mathrm{PH}][\mathrm{H}^+]}{[\mathrm{PH}_2]} \\ K_{\mathrm{P}_2} &= \frac{[\mathrm{P}][\mathrm{H}^+]}{[\mathrm{PH}]} \\ K_{\mathrm{L}_1} &= \frac{[\mathrm{LH}][\mathrm{H}^+]}{[\mathrm{LH}_2]} \\ K_{\mathrm{L}_2} &= \frac{[\mathrm{L}][\mathrm{H}^+]}{[\mathrm{LH}]} \end{aligned} \tag{2}$$

The total concentrations of protein and ligand are:

$$\left[\mathrm{P}^0\right] = [\mathrm{PH}_2] + [\mathrm{PH}] + [\mathrm{P}] \text{ and } \left[\mathrm{L}^0\right] = [\mathrm{LH}_2] + [\mathrm{LH}] + [\mathrm{L}] \tag{3}$$

Using the above relations, one can express all concentrations by the total concentrations and the ionization constants. Therefore, for this reaction scheme the bimolecular association rate constant, k_{R}, can be obtained from the relation:

$$\begin{aligned} k_{\mathrm{R}}\left[\mathrm{P}^0\right]\left[\mathrm{L}^0\right] = {} & k_{\mathrm{R}}^{\mathrm{A}_1}[\mathrm{PH}_2][\mathrm{LH}_2] + k_{\mathrm{R}}^{\mathrm{A}_2}[\mathrm{PH}_2][\mathrm{LH}] + k_{\mathrm{R}}^{\mathrm{A}_3}[\mathrm{PH}_2][\mathrm{L}] \\ & + k_{\mathrm{R}}^{\mathrm{B}_1}[\mathrm{PH}][\mathrm{LH}_2] + k_{\mathrm{R}}^{\mathrm{B}_2}[\mathrm{PH}][\mathrm{LH}] + k_{\mathrm{R}}^{\mathrm{B}_3}[\mathrm{PH}][\mathrm{L}] \\ & + k_{\mathrm{R}}^{\mathrm{C}_1}[\mathrm{P}][\mathrm{LH}_2] + k_{\mathrm{R}}^{\mathrm{C}_2}[\mathrm{P}][\mathrm{LH}] + k_{\mathrm{R}}^{\mathrm{C}_3}[\mathrm{P}][\mathrm{L}] \end{aligned} \tag{4}$$

which can be formulated as:

$$\begin{aligned} k_{\mathrm{R}} = {} & \frac{k_{\mathrm{R}}^{\mathrm{A}_1}}{\left(1+\frac{K_{\mathrm{P}_1}}{[\mathrm{H}^+]}+\frac{K_{\mathrm{P}_1}K_{\mathrm{P}_2}}{[\mathrm{H}^+]^2}\right)\left(1+\frac{K_{\mathrm{L}_1}}{[\mathrm{H}^+]}+\frac{K_{\mathrm{L}_1}K_{\mathrm{L}_2}}{[\mathrm{H}^+]^2}\right)} \\ & + \frac{k_{\mathrm{R}}^{\mathrm{A}_2}}{\left(1+\frac{K_{\mathrm{P}_1}}{[\mathrm{H}^+]}+\frac{K_{\mathrm{P}_1}K_{\mathrm{P}_2}}{[\mathrm{H}^+]^2}\right)\left(1+\frac{K_{\mathrm{L}_2}}{[\mathrm{H}^+]}+\frac{[\mathrm{H}^+]}{K_{\mathrm{L}_1}}\right)} \\ & + \frac{k_{\mathrm{R}}^{\mathrm{A}_3}}{\left(1+\frac{K_{\mathrm{P}_1}}{[\mathrm{H}^+]}+\frac{K_{\mathrm{P}_1}K_{\mathrm{P}_2}}{[\mathrm{H}^+]^2}\right)\left(1+\frac{[\mathrm{H}^+]^2}{K_{\mathrm{L}_1}K_{\mathrm{L}_2}}+\frac{[\mathrm{H}^+]}{K_{\mathrm{L}_2}}\right)} \\ & + \frac{k_{\mathrm{R}}^{\mathrm{B}_1}}{\left(1+\frac{K_{\mathrm{P}_2}}{[\mathrm{H}^+]}+\frac{[\mathrm{H}^+]}{K_{\mathrm{P}_1}}\right)\left(1+\frac{K_{\mathrm{L}_2}}{[\mathrm{H}^+]}+\frac{K_{\mathrm{L}_1}K_{\mathrm{L}_2}}{[\mathrm{H}^+]^2}\right)} \\ & + \frac{k_{\mathrm{R}}^{\mathrm{B}_2}}{\left(1+\frac{K_{\mathrm{P}_2}}{[\mathrm{H}^+]}+\frac{[\mathrm{H}^+]}{K_{\mathrm{P}_1}}\right)\left(1+\frac{K_{\mathrm{L}_2}}{[\mathrm{H}^+]}+\frac{[\mathrm{H}^+]}{K_{\mathrm{L}_1}}\right)} \\ & + \frac{k_{\mathrm{R}}^{\mathrm{B}_3}}{\left(1+\frac{K_{\mathrm{P}_2}}{[\mathrm{H}^+]}+\frac{[\mathrm{H}^+]}{K_{\mathrm{P}_1}}\right)\left(1+\frac{[\mathrm{H}^+]^2}{K_{\mathrm{L}_1}K_{\mathrm{L}_2}}+\frac{[\mathrm{H}^+]}{K_{\mathrm{L}_2}}\right)} \\ & + \frac{k_{\mathrm{R}}^{\mathrm{C}_1}}{\left(1+\frac{[\mathrm{H}^+]^2}{K_{\mathrm{P}_1}K_{\mathrm{P}_2}}+\frac{[\mathrm{H}^+]}{K_{\mathrm{P}_2}}\right)\left(1+\frac{K_{\mathrm{L}_1}}{[\mathrm{H}^+]}+\frac{K_{\mathrm{L}_1}K_{\mathrm{L}_2}}{[\mathrm{H}^+]^2}\right)} \\ & + \frac{k_{\mathrm{R}}^{\mathrm{C}_2}}{\left(1+\frac{[\mathrm{H}^+]^2}{K_{\mathrm{P}_1}K_{\mathrm{P}_2}}+\frac{[\mathrm{H}^+]}{K_{\mathrm{P}_2}}\right)\left(1+\frac{K_{\mathrm{L}_2}}{[\mathrm{H}^+]}+\frac{[\mathrm{H}^+]}{K_{\mathrm{L}_1}}\right)} \\ & + \frac{k_{\mathrm{R}}^{\mathrm{C}_3}}{\left(1+\frac{[\mathrm{H}^+]^2}{K_{\mathrm{P}_1}K_{\mathrm{P}_2}}+\frac{[\mathrm{H}^+]}{K_{\mathrm{P}_2}}\right)\left(1+\frac{[\mathrm{H}^+]^2}{K_{\mathrm{L}_1}K_{\mathrm{L}_2}}+\frac{[\mathrm{H}^+]}{K_{\mathrm{L}_2}}\right)} \end{aligned} \tag{5}$$

For the dissociation process, as a first approximation it can be assumed that the stability of the complex depends on its total electrostatic charge. Therefore five forms of the complex were considered: PLH_4, PLH_3, PLH_2, PLH, and PL, realized by one, four, six, four, and one microscopic states, respectively. In a more realistic model it should be taken into account that each of these microscopic states consistent with a given macrostate can be characterized by different dissociation rate constants. However, available experimental data are not sufficient to consider such details in a reliable way. It should be also noted that not all protonation microstates consistent with the macrostates defined above are substantially populated in the pH range employed in this study, as can be concluded on the basis of theoretical predictions of the pK_{a} values described below. The proton dissociation constants consistent with the above assumptions are:

$$\begin{aligned} K_{\mathrm{C}_1} &= \frac{[\mathrm{PLH}_3][\mathrm{H}^+]}{[\mathrm{PLH}_4]} \\ K_{\mathrm{C}_2} &= \frac{[\mathrm{PLH}_2][\mathrm{H}^+]}{[\mathrm{PLH}_3]} \\ K_{\mathrm{C}_3} &= \frac{[\mathrm{PLH}][\mathrm{H}^+]}{[\mathrm{PLH}_2]} \\ K_{\mathrm{C}_4} &= \frac{[\mathrm{PL}][\mathrm{H}^+]}{[\mathrm{PLH}]} \end{aligned} \tag{6}$$

and the total concentration of the complex is:

$$[\mathrm{C}] = [\mathrm{PLH}_4] + [\mathrm{PLH}_3] + [\mathrm{PLH}_2] + [\mathrm{PLH}] + [\mathrm{PL}] \tag{7}$$

Again, the above equations allow one to express concentrations of all the protonation forms of the complex by [C] and the proton dissociation constants K_{Ci}, and the overall dissociation rate constant can be obtained from the relation:

$$\begin{aligned} k_{\mathrm{D}}[\mathrm{C}] = {} & k_{\mathrm{D}}^{\mathrm{A}_1}[\mathrm{PLH}_4] + \left(k_{\mathrm{D}}^{B_1} + k_{\mathrm{D}}^{\mathrm{A}_2}\right)[\mathrm{PLH}_3] + \\ & \left(k_{\mathrm{D}}^{\mathrm{C}_1} + k_{\mathrm{D}}^{\mathrm{B}_2} + k_{\mathrm{D}}^{\mathrm{A}_3}\right)[\mathrm{PLH}_2] + \left(k_{\mathrm{D}}^{\mathrm{C}_2} + k_{\mathrm{D}}^{\mathrm{B}_3}\right)[\mathrm{PLH}] + k_{\mathrm{D}}^{\mathrm{C}_3}[\mathrm{PL}] \end{aligned} \tag{8}$$

which leads to:

$$k_D = \frac{k_D^{A_1}}{1+\frac{K_{C_1}}{[H^+]}+\frac{K_{C_1}K_{C_2}}{[H^+]^2}+\frac{K_{C_1}K_{C_2}K_{C_3}}{[H^+]^3}+\frac{K_{C_1}K_{C_2}K_{C_3}K_{C_4}}{[H^+]^4}} + \frac{\left(k_D^{B_1}+k_D^{A_2}\right)}{1+\frac{[H^+]}{K_{C_1}}+\frac{K_{C_2}}{[H^+]}+\frac{K_{C_2}K_{C_3}}{[H^+]^2}+\frac{K_{C_2}K_{C_3}K_{C_4}}{[H^+]^3}} + \frac{\left(k_D^{C_1}+k_D^{B_2}+k_D^{A_3}\right)}{1+\frac{[H^+]}{K_{C_2}}+\frac{K_{C_3}}{[H^+]}+\frac{[H^+]^2}{K_{C_1}K_{C_2}}+\frac{K_{C_3}K_{C_4}}{[H^+]^2}} + \frac{\left(k_D^{C_2}+k_D^{B_3}\right)}{1+\frac{[H^+]}{K_{C_3}}+\frac{K_{C_4}}{[H^+]}+\frac{[H^+]^2}{K_{C_2}K_{C_3}}+\frac{[H^+]^3}{K_{C_1}K_{C_2}K_{C_3}}} + \frac{k_D^{C_3}}{1+\frac{[H^+]}{K_{C_4}}+\frac{[H^+]^2}{K_{C_3}K_{C_4}}+\frac{[H^+]^3}{K_{C_2}K_{C_3}K_{C_4}}+\frac{[H^+]^4}{K_{C_1}K_{C_2}K_{C_3}K_{C_4}}} \quad (9)$$

Therefore only five values of the dissociation rate constants can be derived from the pH dependence of the kinetics of dissociation. This is a direct consequence of the simplifying assumption formulated above.

Structures used in calculations

Besides the reaction scheme presented in Fig. 1, the interpretation of the observed pH dependence of the association and dissociation rate constants is also based on a theoretical method for prediction of protonation equilibria in proteins (Antosiewicz et al. 1996; Briggs and Antosiewicz 1999). This method uses molecular structural data at atomic resolution. Our calculations employed the crystal structure of truncated murine eIF4E(28–217) (Marcotrigiano et al. 1997), complexed with m^7GDP, available under access code 1ej1 from the Protein Data Bank (PDB) (Bernstein et al. 1977), and corresponds to the protein used in our experiments. Figure 2 presents a ribbon model of eIF4E complexed with m^7GDP, shown in a CPK representation. Two titratable residues, Glu103 interacting with the N1 and N2 regions of the alkylated base and Lys162 interacting with the phosphate moiety of the ligand, are shown in ball-and-stick representation. The model of m^7GTP was prepared from the m^7GDP structure in the original PBD file, using the program CHARMM (Brooks et al. 1983), with orientation of the γ-phosphate group of the m^7GTP established by 500 steps of steepest descent minimization. Three variants of the model of m^7GTP were considered, resulting from binding the γ-phosphate to three possible oxygen atoms of the β-phosphate of m^7GDP: O1B, O2B, and O3B. This was necessary because minimization of the resulting structure of the m^7GTP was done in the complex with eIF4E, and the additional phosphate group had no full conformational freedom with respect to rotation around the oxygen-phosphorus bond. The model for m^7GMP was derived from the structural data for m^7GDP simply by removing coordinates of the β-phosphate group, followed by 50 steps of steepest descent and 20 steps of conjugate gradient minimization of the region surrounding the removed β-phosphate group.

The coordinate file of Marcotrigiano et al. (1997) contains no hydrogen atoms. For the purpose of calculations in this paper, all hydrogens were added using a HBUILD command of CHARMM (Brunger and Karplus 1988), separately for the apo form of the protein and for each complex with a cap analog. Orientations of added hydrogens were subsequently optimized by 500 steepest descent steps using CHARMM (Brooks et al. 1983).

Electrostatic energies and prediction of protonation states

Prediction of protonation states of titratable residues in the apo form of the eIF4E protein, and in eIF4E complexes with the three

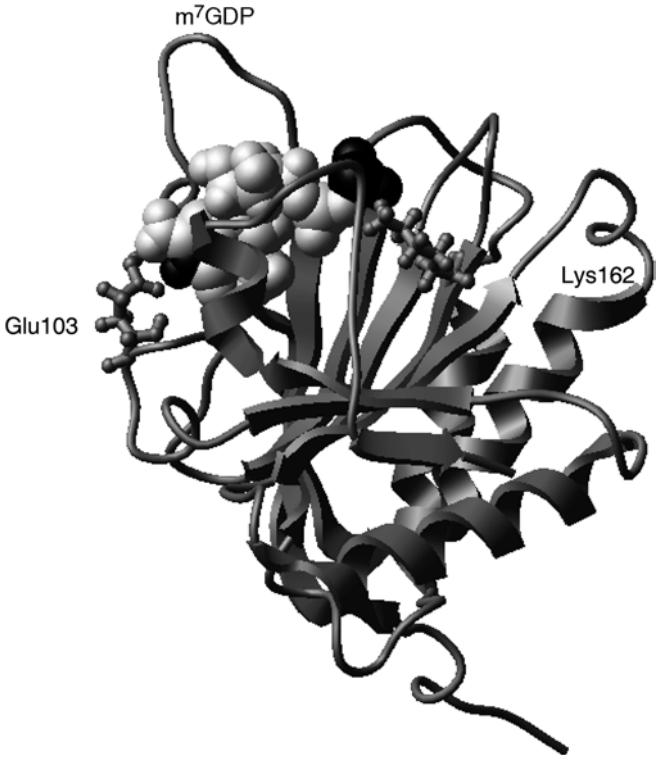

Fig. 2 Structure of murine eIF4E complexed with m^7GDP (prepared using RasMol v2.7.2.1 software written by R. Sayle). The ligand is shown in a *CPK representation*; the protein is shown in *ribbon representation*, with two titratable amino acids, Glu103 and Lys162, shown in *ball-and-stick representation*. The N1-H and the β-phosphate group of the ligand are distinguished by a *black color*

cap analogs, was done as described in detail elsewhere (Antosiewicz et al. 1996; Briggs and Antosiewicz 1999), using the University of Houston Brownian Dynamics program (UHBD) (Davis et al. 1991; Madura et al. 1995) for computing necessary electrostatic free energy interaction matrices, and the HYBRID program (Gilson 1993) to compute titration curves for the titratable residues from the interaction matrix. Our approach is based on the assumption that the difference in protonation behavior of a given group, in the isolated sub-unit and in the biopolymer environment, results exclusively from differences in electrostatic interactions in the two situations. The required electrostatic calculations were performed using the finite-difference Poisson-Boltzmann (PB) method (Warwicker and Watson 1982). The PB model for macromolecular electrostatics treats the solute as a low-dielectric region bounded by the molecular surface, and containing point charges located at the atomic positions determined by X-ray crystallography. The solute is surrounded by a high-dielectric aqueous solvent which may contain a dissolved electrolyte.

Parameters and other details of the simulations

All simulations were performed at 293 K ($RT = 0.58$ kcal/mol), at ionic strengths equivalent to 150 mM monovalent salt, with a solvent dielectric constant of 80 and that for the protein of 4. The dielectric boundary between the protein and the solvent is defined as a Richards probe-accessible surface (Richards 1977) with a 1.4 Å probe radius and an initial set of 280 surface dots per atom (Gilson et al. 1988). All atomic partial charges and radii for the protein were taken from the CHARMM27 parameter set for the standard amino acids and nucleic acids (MacKerell et al. 1998; Foloppe and

MacKerell 2000). Only data for 7-methylguanine with a deprotonated N1 site could not be established with use of these parameter sets. Charge distribution for this case was approximated by assuming that partial charges of N1, C6, and C2 are –0.68, 0.34, and 0.55, respectively, instead of –0.34, 0.54, and 0.75 plus 0.26 for the proton at N1, originally assigned to these atoms in the protonated state of N1. This appears sufficient as a first approximation, and the large upper shift of the pK_a value in the complex with eIF4E (see below) is insensitive to the details of these charges.

Results

Rate constants derived from stopped-flow experiments

Formation of a complex between eIF4E and cap analogs leads to a decrease in intensity of the protein's tryptophan fluorescence, due to quenching processes (Carberry et al. 1989). Figure 3 presents an example of the kinetic traces obtained after mixing solutions of eIF4E and m^7GMP, and the results of application of our fitting procedure to these data. The left side of Fig. 4 shows association rate constants, and the right side shows dissociation rate constants, for the three cap analogs as functions of the pH. The indicated error bars correspond to a 95% confidence level.

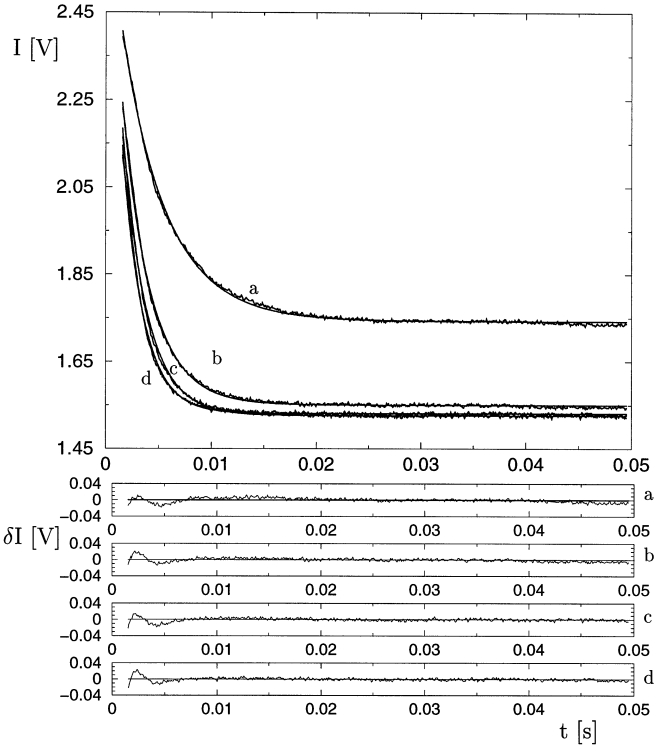

Fig. 3 *Top*: example of kinetic traces obtained after mixing equal volumes of a 1 μM solution of eIF4E with m^7GMP, at concentrations of 4 (*a*), 8 (*b*), 10 (*c*), and 12 (*d*) μM, respectively, at 293 K, pH 7.2, and ionic strength of 150 mM. *Lines without noise* show the simultaneous least-squares fits to the four traces. *Bottom*: four deviations between experimental data and the fits

Predicted ionization constants

Table 1 presents pK_a values for Glu103 and Lys162 in eIF4E and the N1 and terminal phosphate groups in the cap analogs, in isolated states in solution and in complex with each other. The data for the ligands are either experimental values or were approximated to on the basis of experimental data for similar compounds, as described in the Methods section. The remaining data are predictions obtained with the software described above. It should be noted that prediction of ionization constants was done for all titratable residues in the investigated systems. For all the titratable residues not mentioned above, except Arg157, the predicted pK_a values in the apo-protein and in the complexed protein differed by less than 0.2 pH unit. In the case of Arg157, the differences were up to 2 pH units, but all the values were well above the pH range studied in this work.

Association and dissociation rates for different protonation states of the protein and ligand

For each cap analog used in the present study, the nine partial rate constants for the association process listed in Eq. 5 were estimated on the basis of a least-squares method fitting of this equation to the experimental data shown in the left-hand side of Fig. 4. Similarly, the five partial rate constants for the dissociation process, listed in Eq. 9, were obtained by a least-squares method fitting of this equation to the experimental data shown in the right-hand side of Fig. 4. In all these fittings, the pK_a values presented in Table 1, and present in Eq. 5 or 9, were used as fixed parameters of the model. Continuous lines in Fig. 4 present the fits. The partial rate constants, resulting from the fits, are shown in Tables 2 and 3, and Fig. 5 shows fractions of the protein-ligand pairs (left side) and the complex (right side), respectively, in the appropriate protonation state, as functions of pH.

Discussion

Rate constants derived from stopped-flow experiments

It can be seen in Fig. 4 that the pH dependence of the observed overall association rate constants is similar to a bell shape frequently registered for the pH dependence of enzyme kinetics. The entire peaks of these bell-shape dependencies are shifted toward more basic pH values with an increasing number of phosphate groups in the cap analog. The overall dissociation rate constants exhibit some pH dependence for m^7GMP and m^7GDP. The dissociation rate constants are pH independent above pH 6.5, and there is a slight increase in the dissociation rate constants observed when decreasing the pH below value of 6. For m^7GTP, no pH dependence is visible, although there is a large scatter of the data. For m^7GTP the association process is the fastest, and a

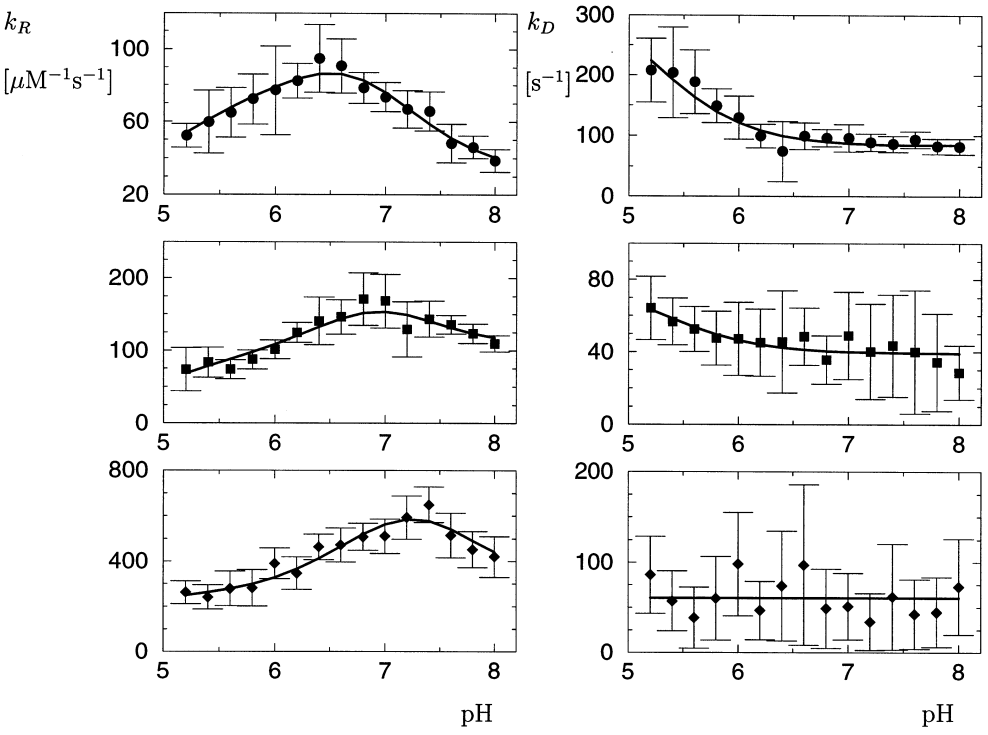

Fig. 4 pH dependence of the association (*left side*) and dissociation (*right side*) rate constants, *top row* for m^7GMP, *middle row* for m^7GDP, and *bottom row* for m^7GTP. The *lines* represent least-squares fits of Eq. 5 for association, and Eq. 9 for dissociation, to the experimental data

Table 1 Predicted and experimental ionization constant data for Glu103 and Lys162 of eIF4E protein, and N1 and terminal phosphate of the cap analogs, at 293 K, ionic strength 150 mM, in free forms and in the complexes. The experimental pK_a values for the free cap analogs are evaluated on the basis of published data (Rhoads et al. 1983; Saenger 1984; Darżynkiewicz et al. 1988; Wieczorek et al. 1995)

Titration site	Free molecules	In the complex
eIF4E and m^7GMP		
Glu103	4.9	0.2
Lys162	6.7	10.9
N1	7.2	18.3
P_α	6.5	5.2
eIF4E and m^7GDP		
Glu103	4.9	0.3
Lys162	6.7	14.9
N1	7.3	18.1
P_β	7.0	5.3
eIF4E and m^7GTP (O3B)		
Glu103	4.9	0.4
Lys162	6.7	14.3
N1	7.4	18.5
$P\gamma$	7.5	7.4
eIF4E and m^7GTP (O2B)		
Glu103	4.9	0.4
Lys162	6.7	18.8
N1	7.4	17.9
$P\gamma$	7.5	12.1
eIF4E and m^7GTP (O1B)		
Glu103	4.9	0.4
Lys162	6.7	14.0
N1	7.4	18.6
$P\gamma$	7.5	12.9

significant part of the process is not available for observation because it occurs within the dead time of our stopped-flow instrument. Consequently, the measured values of the dissociation rate constants for m^7GTP are less accurate.

Table 2 Values of the partial association rate constants, $k_R^{X_i}$ (units of μM^{-1} s^{-1}; see Eq. 5) between different protonation forms of eIF4 and the cap analogs, obtained from fitting Eq. 5 to data presented on the left side of Fig. 4

Protein:ligand protonation form	$k_R^{X_i}$			Fraction line code in Fig. 5
	m^7GMP	m^7GDP	m^7GTP	
P2H:L2H	10	10	200	Thick solid
P2H:L1H	nr[a]	nr	nr	Negligible fraction
P2H:L0H	nr	nr	nr	Negligible fraction
P1H:L2H	70	90	230	Thick dashed
P1H:L1H	110	250	1600	Thick long-dashed
P1H:L0H	300	230	2250	Thick dot-dashed
P0H:L2H	15	140	460	Thin dashed
P0H:L1H	10	140	500	Thin long-dashed
P0H:L0H	30	100	300	Thin dot-dashed

[a]nr = not reliable, because the fraction of the protein ligand pairs is negligibly small in the investigated pH range

Predicted ionization constants

According to the data presented in Table 1, in the uncomplexed protein, pK_a values for Glu103 and Lys162 are 4.9, and 6.7, respectively. On the other hand, the uncomplexed ligand has pK_a values of ~7.3 at the N1 position, and the pK_a of the secondary ionization of the terminal phosphate group changes from 6.5 in m^7GMP, through 7.0 for m^7GDP, to 7.5 for m^7GTP. Therefore these four titratable sites can influence the pH dependence of the association rate constant. On the other

Table 3 Values of the partial dissociation rate constants, $k_D^{X_i}$ (units of s^{-1}; see Eq. 9) for different protonation forms of eIF4 and the cap analog complexes, obtained from fitting Eq. 9 to data presented on the right side of Fig. 4

Protonation form of complex	$k_R^{X_i}$			Fraction line code in Fig. 5
	m^7GMP	m^7GDP	m^7GTP	
PLH_4	nr[a]	nr	nr	Negligible fraction
PLH_3	370	80	60	Thick dashed
PLH_2	80	40	nr	Thick long-dashed[b]
PLH	nr	nr	nr	Negligible fraction
PL	nr	nr	nr	Negligible fraction

[a]nr = not reliable, because the fraction of the protein ligand pairs is negligibly small in the investigated pH range
[b]Negligible fraction for m^7GTP-eIF4E complex

hand, in the complex the above ionization equilibria are shifted owing to mutual interactions and changes in the molecular environment. The pK_a of Glu103 is significantly shifted down, below the lowest pH considered in this study, in all the complexes. Therefore one can expect that the protonation equilibrium of Glu103 would not influence the observed pH dependence of the dissociation rate constants. The pK_a of Lys162 is shifted upward in all cases: to the value of 10.9 in the complex with m^7GMP and to >14 for the complexes with m^7GDP and m^7GTP. Our pK_a predictions for eIF4E-m^7GMP, without minimization of the structure of the complex after removal of the β-phosphate group from the original crystal structure data, give pK_a values of 9.3 for the α-phosphate and of 8.0 for Lys162. These results are not compatible with the experimental data for the dissociation rate constant for the eIF4E-m^7GMP complex, because in this case some pH dependence of the dissociation rate constants would be observed on the alkaline side of the investigated pH range, rather than on the acidic side. This indicates that, locally, the structure of the protein is different in the complex with the monophosphate analog as compared to the diphosphate analog, and the change is in a direction to allow for stronger interaction between the α-phosphate and Lys162. The pK_a values at N1 of the ligands are all significantly shifted upwards, because of strong electrostatic interaction with the negatively charged Glu103. Finally, different shifts in the pK_a values for secondary ionization of the phosphate group are predicted for the three cap analogs. For m^7GMP and m^7GDP there is a shift to lower values, because of interaction with Lys162, stabilizing the dianion form of the terminal phosphate. However, for m^7GTP, two different pK_a values for the secondary ionization are predicted, depending on the oxygen atom to which the group is attached during modeling. When the γ-phosphate is bound to oxygen O3B, the predicted pK_a is almost the same as in the free molecule, because in this case the terminal phosphate is exposed to solvent. For the two remaining possibilities, the pK_a values are shifted to a pH about 12, probably because in the vicinity of the γ-phosphate there is no positively charged group which could stabilize the dianion form of the phosphate. However, when the γ-phosphate is attached to the oxygen atom O2B, there is an additional electrostatic stabilization of the protonated form of Lys162, as its pK_a value is increased by a further 4 pH units, relative to the two remaining cases (see Table 1). This structure was assumed to be the most probable for further discussion.

From comparisons between experimental and predicted pK_a values in previous studies (Antosiewicz et al.

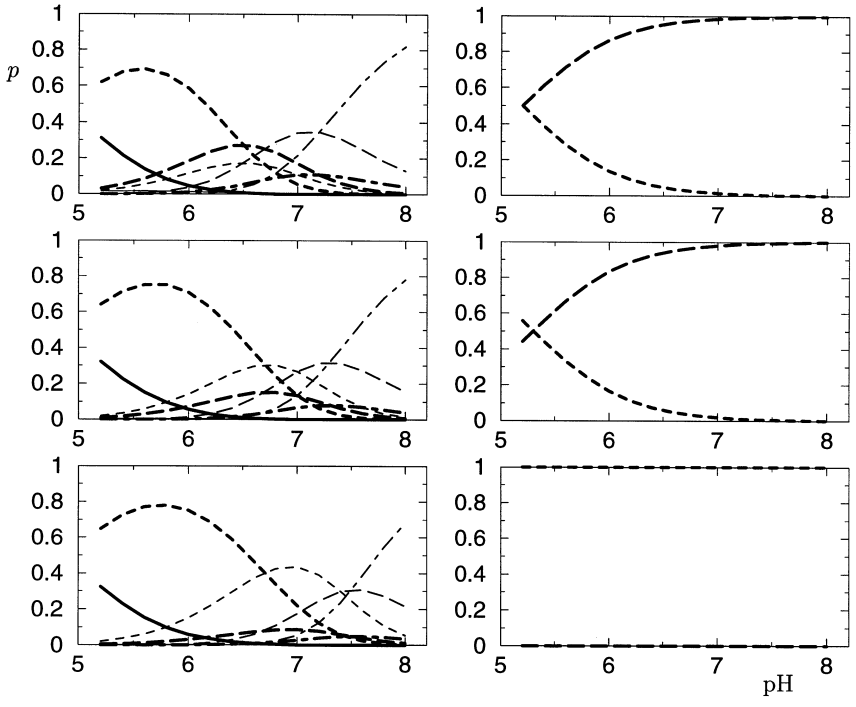

Fig. 5 Fractions of protein:ligand pairs with a given protonation pattern, shown in Fig. 1, as functions of pH. *Left side*: P2H:L2H, *thick solid line*; P1H:L2H, *thick dashed line*; P1H:L1H, *thick long-dashed line*; P1H:L0H, *thick dot-dashed line*; P0H:L2H, *thin dashed line*; P0H:L1H, *thin long-dashed line*; P0H:L0H, *thin dot-dashed line*. *Right side*: PLH_3, *thick dashed line*; PLH_2, *thick long-dashed line*. Populations not shown are negligibly small. *Top row* is for m^7GMP, *middle row* for m^7GDP, and *bottom row* for m^7GTP

1996; Briggs and Antosiewicz 1999), we can expect that the accuracy of the present predictions should not be worse than ±0.8 pH unit. Therefore the data presented in Table 1 indicate that we can expect some influence of all four ionizations on the binding process, and that only ionizations of the phosphates in the complex will be visible in the dissociation process for the complexes with m^7GMP and m^7GDP, but the dissociation rate constant for m^7GTP should be pH independent in the range studied in this work. It should be remembered that these conclusions are valid provided that the establishment of the protonation equilibrium for all molecular species in solution is fast in comparison to the process of formation and dissociation of the complex, as implicitly assumed in the reaction scheme presented in Fig. 1. As is seen in Fig. 2, the titratable groups discussed here are close to the molecular surface; therefore it can be expected that protonation/deprotonation reactions of these sites are sufficiently fast.

Consistency of the experimental observations with theoretical predictions

The continuous lines in Fig. 4 indicate that the experimental observations can be reasonably reproduced by our model. Although the rate constants obtained from our stopped-flow experimental data are subject to quite substantial statistical error, the data presented in Tables 2 and 3 have at least a semi-quantitative value. These data are the result of our least-squares fits with all nine rate constants for association and all five rate constants for dissociation reactions. It should be analyzed together with the results presented in Fig. 5. If the fraction of a given protonation form is negligible in the investigated pH range, then the corresponding rate constant, obtained from the fitting, is not meaningful because the program usually leaves the corresponding rate constant close to its starting value; this is indicated in Tables 2 and 3 as "nr" (not reliable). It is clear from Eqs. 5 and 9 that if the fraction of molecular species with a given protonation pattern is practically zero, the contribution of this species to the observed rate constant is negligible. Also it may be possible that the two particularly large values for the association rate constants obtained for m^7GTP, for protonation forms P1H:L1H and P1H:L0H, are so large because populations of the corresponding molecular species, while not negligible, are nevertheless very small (see Fig. 5). However, all values presented in Tables 2 and 3 are reproducible within ±20%, for different sets of starting values, leading to fits of comparable quality. Therefore we believe that they have some significance and, based on these data, reliable conclusions can be made. One of them is related to the protonation state at the N1 position of the ligand required for effective protein-ligand recognition and after formation of the complex, discussed already in the Introduction section. From the data presented in Table 2 it may be concluded that both protonation forms of the ligand, as regards its N1 position, are recognized by the eIF4E binding site. This conclusion is based on two facts. First, setting the three partial rate constants to zero for the L2H form of the ligand (for its binding to P2H, P1H, and P0H forms of the protein), and keeping them fixed at these values during fitting, or doing analogously for the L0H form of the ligand, leads to a substantial increase in the RMS deviation for the best fit of Eq. 5 to the experimental data shown in the left-hand side of Fig. 4. Second, it can be seen in Table 2 that the association rate constants obtained for the ligand with two protons attached are comparable to the association rate constants obtained for the ligand with the two protons dissociated.

Conclusions

In this study we have analyzed, by investigation of pH effects, the role played by two residues in the binding site of eIF4E (Glu103 and Lys162) and N1 and the terminal phosphate in the cap analog in the association process. We have shown that protonation equilibria of these four sites influences the initial steps in complex formation. Predicted pK_a values for the free protein and ligand are consistent with the observed pH dependence of the association rate constant. Our data indicate that both protonation forms of the cap analogs, regarding the N1 position of the guanine ring, are recognized by the binding site of the eIF4E protein. After formation of the complex, the protonation equilibria of the four sites are changed, resulting in an electrostatic stabilization of the complex, and again the predicted shifts in the pK_a values of the four groups are consistent with the experimental data obtained from our stopped-flow experiments. These electrostatic effects, due to the participation of the titratable groups in the binding, emerging from the present study, appear to be additional elements supplementing the mechanism of eIF4E-cap recognition involving stacking interactions between the methylated guanine ring and the two conserved tryptophan residues described by others (Marcotrigiano et al. 1997; Matsuo et al. 1997).

Acknowledgements We thank Prof. D. Shugar for reading the manuscript and useful comments, and anonymous referees for valuable suggestions. This work was supported by the State Committee for Scientific Research (KBN) (grants 6-P04A-055-17 and 8-T11F-016-16).

References

Adams JA, Taylor SS (1993) Phosphorylation of peptide substrates for the catalytic subunit of cAMP-dependent protein kinase. J Biol Chem 268:7747–7752

Antosiewicz J, Briggs JM, Elcock AE, Gilson MK, McCammon JA (1996) Computing the ionization states of proteins with a detailed charge model. J Comput Chem 17:1633–1644

Bernstein FC, Koettzle TF, Williams GJB, Meyer EF, Brice MD, Rodgers JR, Kennard O, Shimanouchi T, Tasumi MJ (1977)

The protein data bank: a computer-based archival file for molecular structures. J Mol Biol 123:557–594

Brendskag MK, McKinley-McKee JS, Winberg J (1999) *Drosphila lebanonesis* alcohol dehydrogenase: pH dependence of the kinetic coefficients. Biochim Biophys Acta 1431:74–86

Briggs JM, Antosiewicz J (1999) Simulation of pH-dependent properties of proteins using mesoscopic models. Rev Comput Chem 13:249–311

Brooks BR, Bruccoleri RE, Olafson BD, States DJ, Swaminathan S, Karplus M (1983) CHARMM: a program for macromolecular energy, minimization, and dynamics calculations. J Comput Chem 4:187–217

Brunger AT, Karplus M(1988) Polar hydrogen positions in proteins: empirical energy placement and neutron diffraction comparison. Proteins Struct Funct Genet 4:148–156

Carberry SE, Rhoads RE, Goss DJ (1989) A spectroscopic study of binding of m7GTP and m7GpppG to human protein synthesis initiation factor 4E. Biochemistry 28:8078–8082

Cleland WW (1982) The use of pH studies to determine chemical mechanisms of enzyme-catalyzed reactions. Methods Enzymol 87:390–405

Darżynkiewicz E, Ekiel I, Tahara SM, Seliger LS, Shatkin AJ (1985) Chemical synthesis and characterization of 7-methylguanosine cap analogues. Biochemistry 24:1701–1707

Darżynkiewicz E, Labadi I, Haber D, Burger K, Lönnberg H (1988) 7-Methylguanine nucleotides and their structural analogues; protolytic equilibria, complexing with magnesium(II) ion and kinetics for alkaline opening of the imidazole ring. Acta Chem Scand B 42:86–92

Davis ME, Madura JD, Luty BA, McCammon JA (1991) Electrostatics and diffusion of molecules in solution: simulations with the University of Houston Brownian Dynamics program. Comput Phys Commun 62:187–197

Długosz M, Bojarska E, Antosiewicz JM (2002) A procedure for analysis of stopped-flow transients for protein-ligand association. J Biochem Biophys Methods 51:179–193

Foloppe N, MacKerell AD Jr (2000) All-atom empirical force field for nucleic acids. I. Parameter optimization based on small molecule and condensed phase macromolecular target data. J Comput Chem 21:86–104

Gilson MK (1993) Multiple-site titration and molecular modeling: two rapid methods for computing energies and forces for ionizable groups in proteins. Proteins Struct Funct Genet 15:266–282

Gilson MK, Sharp KA, Honig BH (1988) Calculating the electrostatic potential of molecules in solution: method and error assessment. J Comput Chem 9:327–335

Johnson KA (1992) Transient-state kinetic analysis of enzyme reaction pathways. Enzymes 20:1–61

Kitano H, Maeda Y, Okubo T (1989) Kinetic study of the effects of solvation on the dimerization process of α-chymotrypsin. Biophys Chem 33:47–54

MacKerell AD Jr, Bashford D, Bellott M, Dunbrack RL Jr, Evanseck JD, Field MJ, Fischer S, Gao J, Guo H, Ha S, Joseph-McCarthy D, Kuchnir L, Kuczera K, Lau FTK, Mattos C, Michnick S, Ngo T, Nguyen DT, Prodhom B, Reiher WE III, Roux B, Schlenkrich M, Smith JC, Stote R, Straub J, Watanabe M, Wiorkiewicz-Kuczera J, Yin D, Karplus M (1998) All-atom empirical potential for molecular modeling and dynamics studies of proteins. J Phys Chem B 102:3586–3616

Madura JD, Briggs JM, Wade RC, Davis ME, Luty BA, Ilin A, Antosiewicz J, Gilson MK, Bagheri B, Scott LR, McCammon JA (1995) Electrostatics and diffusion of molecules in solution: simulations with the University of Houston Brownian Dynamics program. Comput Phys Commun 91: 57–95

Marcotrigiano J, Gingras A, Sonenberg N, Burley SK (1997) Cocrystal structure of the messenger RNA 5′ cap-binding protein (eIF4E) bound to 7-methyl-GDP. Cell 89:951–961

Matsuo H, Li H, McGuire AM, Fletcher CM, Gingras A, Sonenberg N, WagnerG (1997) Structure of translation factor eIF4E bound to m7GDP and interaction with 4E-binding protein. Nat Struct Biol 4:717–724

Rhoads RE, Hellmann GM, Remy P, Ebel J (1983) Translational recognition of messenger RNA caps as a function of pH. Biochemistry 22:6084–6088

Richards FM (1977) Areas, volumes, packing and protein structure. Annu Rev Biophys Bioeng 6:151–176

Saenger W (1984). Principles of nucleic acid structure. Springer, Berlin Heidelberg New York

Sonenberg N, Gingras AC (1998) The mRNA 5′ cap-binding protein eIF4E and control of cell growth. Curr Opin Cell Biol 10:268–275

Stivers JT, Abeygunawardana C, Mildvan AS (1996) 4-Oxalocrotonate tautomerase: pH dependence of catalysis and pK_a values of active site residues. Biochemistry 35:814–823

Taylor KC, Vitello LB, Erman JE (2000) 4-Nitroimidazole binding to horse metmyoglobin: evidence for preferential anion binding. Arch Biochem Biophys 382:284–295

Tipton KF, Dixon HBF (1979) Effects of pH on enzymes. Methods Enzymol 63:183–234

Warwicker J, Watson HC (1982) Calculation of the electric potential in the active site cleft due to α-helix dipoles. J Mol Biol 157:671–679

Wieczorek Z, Stepinski J, Jankowska M, Lönnberg H (1995) Fluorescence and absorption spectroscopic properties of RNA 5′-cap analogues derived from 7-methyl-, N^2,7-dimethyl- and N^2,N^2,7-trimethyl-guanosines. J Photochem Photobiol 28:57–63